

EM-WaveHoltz: A flexible frequency-domain method built from time-domain solvers

Zhichao Peng and Daniel Appelö

Abstract—A novel approach to computing time-harmonic solutions of Maxwell’s equations by time-domain simulations is presented. The method, EM-WaveHoltz, results in a positive definite system of equations which makes it amenable to iterative solution with the conjugate gradient method or with GMRES. Theoretical results guaranteeing the convergence of the method away from resonances is presented. Numerical examples illustrating the properties of EM-WaveHoltz are given.

Index Terms—Maxwell equations, iterative method, electrochemical analysis, frequency-domain analysis, time-domain analysis, FDTD methods, discontinuous Galerkin time-domain (DGTD) methods, positive definite

TWO of the main challenges when solving the time-harmonic Maxwell equations at high frequencies are the indefinite nature of the Maxwell system and the high resolution requirement. Without proper preconditioners, iterative solvers such as GMRES and BICG may converge slowly. These challenges are similar to the ones for solving the Helmholtz equation at high frequencies. Recently, we introduced a scalable iterative method called WaveHoltz [1] for the Helmholtz equation. In this paper, we introduce the electromagnetic-WaveHoltz (EM-WaveHoltz) method, which can be seen as a generalization of the WaveHoltz method to the time-harmonic (or frequency-domain) Maxwell equations. The proposed EM-WaveHoltz method converts the frequency-domain problem to a fix point problem in the time-domain. The fixed point iteration is linear and can be rewritten as a linear system of equations with a system matrix that is positive definite and that can therefore be efficiently inverted using standard Krylov methods such as GMRES.

In the EM-WaveHoltz method, we convert the frequency-domain problem to a time-domain problem by evolving and filtering Maxwell’s equations with periodic forcing over one time period. When applied, this filter results in the time-domain solution converging to a fix point where the solution becomes equivalent to the solution of the frequency-domain problem. Salient features of the EM-WaveHoltz method are as follows.

- 1) The resulting linear system is always positive definite (sometimes symmetric).
- 2) The EM-WaveHoltz method can be driven by any scalable time-domain solver, for example the finite difference time-domain (FDTD) method [2] and discontinuous Galerkin time-domain method (DGTD) [3].

- 3) A unique feature of the EM-WaveHoltz method is that it is possible to obtain frequency-domain solutions for multiple frequencies at once but at the cost of a single solve.

We note that properties of our method are to some extent shared with the properties of the controllability method. In particular the controllability method finds the solution to the frequency-domain problem by using time-domain solvers like our approach. However, while our formulation relies on a fixed point iteration, the controllability method seeks to minimize the deviation from time-periodicity of the initial and final data of the time-domain simulation. The controllability method was first proposed for a time-harmonic wave scattering problem [4], and we refer readers to [5] for recent development. The controllability method is also generalized to the time-harmonic Maxwell equation in the second order formulation [6] and the first formulation [7], [8]. One main difference between our method and the controllability method is that the controllability method needs backward solves, while our method does not.

There are of course many other methods that have been designed for efficiently solving the frequency-domain Maxwell’s equations. For scattering and radiation problems in homogeneous media integral equation formulations are known to be highly efficient and yield fast algorithms [9], [10]. Domain decomposition methods (DDM) [11] have also achieved success for the time-harmonic electromagnetic problems [12], [13], [14], [15], [16]. The DDM method and the integral equation method have been combined in [17]. Recently, [18] extends the “shifted-Laplacian preconditioner” for the Helmholtz equation to the high frequency time-harmonic Maxwell equations and designs an optimal DDM method. Multigrid methods have also been considered for the time-harmonic Maxwell equations [19], [20]. A multigrid method for the high frequency time-harmonic Maxwell equations is designed in [21]. Sweeping preconditioners for time-harmonic Maxwell equations, which utilize the intrinsic structure of the Green’s function, have been developed for the Yee scheme [22] and the finite element method [23].

The rest of this paper is organized as follows. In Section I, we present the EM-WaveHoltz formulation for the continuous equations and discuss the properties of the resulting linear system, the choice of the linear solver, and present how to obtain solutions for multiple frequencies in one solve. In Section II, to show the flexibility with respect to the choice of the time-domain solvers, we couple the EM-WaveHoltz method, first with the Yee scheme and then with the discontinuous Galerkin (DG) method. In Section III, the performance of the

Zhichao Peng is with the Department of Mathematics, Michigan State University, East Lansing, MI 48824.

Daniel Appelö is with the Department of Computational Mathematics, Science & Engineering and the Department of Mathematics, Michigan State University, East Lansing, MI 48824

Manuscript received March 1, 2025; revised March 1, 2025.

EM-WaveHoltz method is demonstrated through a series of numerical examples.

I. ELECTROMAGNETIC WAVEHOLTZ ITERATION FOR THE MAXWELL'S EQUATION

We consider the frequency-domain Maxwell's equation:

$$i\omega\epsilon\mathbf{E} = \nabla \times \mathbf{H} - \mathbf{J}, \quad (1a)$$

$$i\omega\mu\mathbf{H} = -\nabla \times \mathbf{E}, \quad (1b)$$

closed by boundary conditions corresponding to either a perfect electric conductor or to an unbounded domain. Here \mathbf{E} and \mathbf{H} are the complex valued electric and magnetic fields and \mathbf{J} is the real valued current source. Taking the real and imaginary parts we find

$$-\omega\Im\{\epsilon\mathbf{E}\} = \Re\{\nabla \times \mathbf{H}\} - \mathbf{J}, \quad (2a)$$

$$\omega\Re\{\epsilon\mathbf{E}\} = \Im\{\nabla \times \mathbf{H}\}, \quad (2b)$$

$$-\omega\Im\{\mu\mathbf{H}\} = -\Re\{\nabla \times \mathbf{E}\}, \quad (2c)$$

$$\omega\Re\{\mu\mathbf{H}\} = -\Im\{\nabla \times \mathbf{E}\}. \quad (2d)$$

We want to relate the fields \mathbf{E} and \mathbf{H} to real valued and $T = 2\pi/\omega$ -periodic solutions

$$\tilde{\mathbf{E}} = \hat{\mathbf{E}}_0 \cos(\omega t) + \hat{\mathbf{E}}_1 \sin(\omega t), \quad (3a)$$

$$\tilde{\mathbf{H}} = \hat{\mathbf{H}}_0 \cos(\omega t) + \hat{\mathbf{H}}_1 \sin(\omega t), \quad (3b)$$

to the time-domain equations

$$\epsilon\partial_t \tilde{\mathbf{E}} = \nabla \times \tilde{\mathbf{H}} - \sin(\omega t)\mathbf{J}, \quad (4a)$$

$$\mu\partial_t \tilde{\mathbf{H}} = -\nabla \times \tilde{\mathbf{E}}. \quad (4b)$$

For such periodic solutions we can match the $\sin(\omega t)$ and $\cos(\omega t)$ terms to find the relations

$$\epsilon\omega(-\hat{\mathbf{E}}_0) = \nabla \times \hat{\mathbf{H}}_1 - \mathbf{J},$$

$$\epsilon\omega(\hat{\mathbf{E}}_1) = \nabla \times \hat{\mathbf{H}}_0,$$

$$\mu\omega(-\hat{\mathbf{H}}_0) = -\nabla \times \hat{\mathbf{E}}_1,$$

$$\mu\omega(\hat{\mathbf{H}}_1) = -\nabla \times \hat{\mathbf{E}}_0.$$

It now follows that the initial data of $\tilde{\mathbf{E}}$ and $\tilde{\mathbf{H}}$ determines the imaginary part of the frequency-domain solution

$$\Im\{\mathbf{E}\} = \hat{\mathbf{E}}_0, \quad \Im\{\mathbf{H}\} = \hat{\mathbf{H}}_0,$$

as well as the real part

$$\Re\{\mathbf{E}\} = \hat{\mathbf{E}}_1 = \frac{1}{\epsilon} \nabla \times \hat{\mathbf{H}}_0, \quad \Re\{\mathbf{H}\} = \hat{\mathbf{H}}_1 = -\frac{1}{\mu} \nabla \times \hat{\mathbf{E}}_0. \quad (5)$$

Our EM-WaveHoltz method finds the periodic solutions (3) by iteratively determining the initial data,

$$\tilde{\mathbf{E}}|_{t=0} = \nu_E = \hat{\mathbf{E}}_0, \quad \tilde{\mathbf{H}}|_{t=0} = \nu_H = \hat{\mathbf{H}}_0,$$

to (4). Define the filtering operator, Π , acting on the initial conditions $\nu = (\nu_E, \nu_H)^T$:

$$\Pi\nu = \Pi \begin{pmatrix} \nu_E \\ \nu_H \end{pmatrix} = \frac{2}{T} \int_0^T \left(\cos(\omega t) - \frac{1}{4} \right) \begin{pmatrix} \tilde{\mathbf{E}} \\ \tilde{\mathbf{H}} \end{pmatrix} dt, \quad (6)$$

with $T = 2\pi/\omega$.

By construction, one can verify that $\Pi(\Im\{\mathbf{E}\}, \Im\{\mathbf{H}\})^T = (\Im\{\mathbf{E}\}, \Im\{\mathbf{H}\})^T$. As the real part can be computed directly via (5), the solution to the frequency-domain equation is a fix-point of the operator Π . Based on these facts, we define the EM-WaveHoltz iteration:

$$\Pi\nu^{n+1} = \Pi\nu^n, \quad \text{with } \nu^0 = (\nu_E^0, \nu_H^0)^T = \mathbf{0}. \quad (7)$$

The EM-WaveHoltz iteration converges to the imaginary parts of the solution to the frequency-domain equation

$$\lim_{n \rightarrow \infty} \nu^n = \lim_{n \rightarrow \infty} (\nu_E^n, \nu_H^n)^T = (\Im\{\mathbf{E}\}, \Im\{\mathbf{H}\})^T, \quad (8)$$

and the real parts can be recovered via (5).

Remark 1. Alternatively we could formulate the time-domain problem with a cosine forcing

$$\epsilon\partial_t \tilde{\mathbf{E}} = \nabla \times \tilde{\mathbf{H}} - \cos(\omega t)\mathbf{J}, \quad (9a)$$

$$\mu\partial_t \tilde{\mathbf{H}} = -\nabla \times \tilde{\mathbf{E}}. \quad (9b)$$

Again, the real valued $T = 2\pi/\omega$ -periodic solutions to (9) are on the form (3) but (see Appendix A) the solution to (9) $\tilde{\mathbf{E}}$ and $\tilde{\mathbf{H}}$ have a slightly different relation to the frequency-domain solution

$$\Re\{E\} = \hat{E}_0, \quad \Re\{H\} = \hat{H}_0, \quad \Im\{E\} = -\hat{E}_1, \quad \Im\{H\} = -\hat{H}_1.$$

With the same filter and iteration process defined as the sin-forcing case, we have

$$\lim_{n \rightarrow \infty} \nu^n = \lim_{n \rightarrow \infty} (\nu_E^n, \nu_H^n)^T = (\Re\{\mathbf{E}\}, \Re\{\mathbf{H}\})^T. \quad (10)$$

In our numerical tests, we find that the number of iterations needed by the EM-WaveHoltz method are essentially identical for the two alternatives. In this paper, we focus on the EM-WaveHoltz with the sin-forcing.

A. EM-WaveHoltz for the energy conserving case

For PEC boundary conditions and other boundary conditions that lead to a conservation of the electromagnetic energy in a bounded domain, the EM-WaveHoltz iteration can be simplified further. For such problems $\Im\{\mathbf{H}\}$ is identically zero and the EM-WaveHoltz iteration is reduced to

$$\nu_E^{n+1} = \Pi\nu_E^n, \quad \nu_H^n = \mathbf{0}, \quad \nu_E^0 = \mathbf{0}, \quad (11)$$

where now

$$\Pi\nu_E = \frac{2}{T} \int_0^T \left(\cos(\omega t) - \frac{1}{4} \right) \tilde{\mathbf{E}} dt. \quad (12)$$

As long as ω is not a resonance this simplified EM-WaveHoltz iteration converges

$$\nu_E^n = \Im\{\mathbf{E}\}, \quad \text{as } n \rightarrow \infty. \quad (13)$$

B. Krylov acceleration

For bounded problems where ω is close to a resonance or for unbounded problems with trapping geometries, the convergence of the WaveHoltz fix point iteration can be slow [1]. Fortunately as the iteration is linear, it is easy to rewrite it as a positive definite linear operator that can be efficiently inverted by a Krylov subspace method. To see this we introduce the operator:

$$S\boldsymbol{\nu} = \Pi\boldsymbol{\nu} - \Pi\mathbf{0}. \quad (14)$$

Then, based on the definition of S , we have

$$\Pi\boldsymbol{\nu} = S\boldsymbol{\nu} + \Pi\mathbf{0}. \quad (15)$$

Hence, finding the fix point of Π : $\Pi\boldsymbol{\nu} = \boldsymbol{\nu}$ is equivalent to solving the equation $(I - S)\boldsymbol{\nu} = \Pi\mathbf{0}$.

A Krylov method such as the conjugate gradient method, GMRES or TFQMR can be applied to solve $(I - S)\boldsymbol{\nu} = \Pi\mathbf{0}$ in a matrix-free manner. In practice, to obtain the right hand side $\Pi\mathbf{0}$, we just need to solve the time-domain problem (4) with zero initial conditions $\boldsymbol{\nu} = \mathbf{0}$ from $t = 0$ to $t = T$ and use a numerical quadrature to approximate the filter $\Pi\mathbf{0}$ as we march in time. To calculate the matrix multiplication $(I - S)\boldsymbol{\nu}$, we can utilize the fact that

$$(I - S)\boldsymbol{\nu} = \boldsymbol{\nu} - (\Pi\boldsymbol{\nu} - \Pi\mathbf{0}) = \boldsymbol{\nu} - \Pi\boldsymbol{\nu} + \Pi\mathbf{0}.$$

That is, for a given $\boldsymbol{\nu}$ and $\Pi\mathbf{0}$ precomputed, we just need to compute $\Pi\boldsymbol{\nu}$ to obtain the action of $(I - S)$ onto $\boldsymbol{\nu}$. Recall that $\Pi\boldsymbol{\nu}$ is obtained by computing the filter by a numerical quadrature incrementally as the solution to (4) is evolved for one $T = 2\pi/\omega$ period with $\boldsymbol{\nu}$ as the initial conditions. Thus the cost to compute one Krylov vector is that of a wave solve with one additional variable needed to sum up the projection throughout the evolution.

When using GMRES there is always a concern about the size of the Krylov subspace as the number of iterations grow. Here our method has a significant upside to solving the frequency-domain problem. Note that although we are looking for a $T = \frac{2\pi}{\omega}$ -periodic solution, there is nothing in the method that prevents us from changing the filtering to extend over a longer time, say, $T = N\frac{2\pi}{\omega}$, with N a positive integer. As we show in the numerical examples below, for moderate N this reduces the number of iterations by a factor of N so that the overall computational cost is the same. However, using a longer iteration with $N > 1$ reduces the size of the GMRES Krylov subspace by a factor of N compared to a frequency-domain iteration.

In Appendix B, we show that $I - S$ is always a positive definite operator and for energy conserving boundary conditions it is also self-adjoint. These results carry over to the discretized equations in the sense that the matrix that needs to be inverted is always positive definite and, if a symmetric and energy conserving method (like the Yee scheme) is used, the matrix is also symmetric for energy conserving boundary conditions like PEC. For the SPD case our method becomes particularly efficient and memory lean as the conjugate gradient method can be used.

C. Multiple frequencies in one solve

Similar to the WaveHoltz method for the Helmholtz equation [1], the EM-WaveHoltz method can be applied to obtain the solutions for multiple frequencies in one solve.

Precisely, let $\omega_k = n_k\omega_0$, $k = 1, \dots, N$ for some $\omega_0 > 0$ and $n_1 < n_2 < \dots < n_N$ being positive integers. Then in a traditional frequency-domain solver each frequency requires the solution of N different systems

$$i\omega_k\epsilon\mathbf{E}_k = \nabla \times \mathbf{H}_k - \mathbf{J}_k, \quad (16a)$$

$$i\omega_k\mu\mathbf{H}_k = -\nabla \times \mathbf{E}_k. \quad (16b)$$

Now, assuming that each frequency solve has the same type of boundary condition and material properties (the forcing \mathbf{J}_k can be different for each k), we can solve for all frequencies at once. We take the energy conserving case as an example, then the **single** time-domain problem we must solve is

$$\epsilon\partial_t\tilde{\mathbf{E}} = \nabla \times \tilde{\mathbf{H}} - \sum_{k=1}^N \sin(\omega_k t)\mathbf{J}_k, \quad (17a)$$

$$\mu\partial_t\tilde{\mathbf{H}} = \nabla \times \tilde{\mathbf{E}}. \quad (17b)$$

The converged solution to (17) can be decomposed as

$$\tilde{\mathbf{E}} = \sum_{k=1}^N \hat{\mathbf{E}}_{k,0} \cos(\omega_k t), \quad (18)$$

where $\hat{\mathbf{E}}_{k,0} = \Im\{\mathbf{E}_k\}$ gives the solution to the original frequency-domain problem (16) corresponding to ω_k . To obtain the “all k ” solution through EM-WaveHoltz is easy, the filtering operator simply needs to be modified as

$$\Pi\boldsymbol{\nu}_E = \frac{2}{T} \int_0^T \left(\sum_{k=1}^N \cos(\omega_k t) - \frac{1}{4} \right) \tilde{\mathbf{E}} dt. \quad (19)$$

Here, the final time T is chosen such that $T/(\frac{2\pi}{\omega_k})$ is an integer for all k .

Once the EM-WaveHoltz iteration has converged to (18) we separate the different solutions by evolving (16) for one more T_k -period while applying the filters

$$\Im(\mathbf{E}_k) = \frac{2}{T_k} \int_0^{T_k} \left(\cos(\omega_k t) - \frac{1}{4} \right) \tilde{\mathbf{E}} dt, \quad (20)$$

$$\Re(\mathbf{E}_k) = \frac{2}{T_k} \int_0^{T_k} \sin(\omega_k t) \tilde{\mathbf{E}} dt. \quad (21)$$

II. DISCRETIZATION OF THE EM-WAVEHOLTZ METHOD

We have presented how the EM-WaveHoltz iteration converts a frequency-domain problem to a time-domain problem. In this section, we will use the Yee scheme [24], [25] and the discontinuous Galerkin (DG) method [3], [26], [27] as examples of integrating the EM-WaveHoltz iteration in existing time-domain solvers. We also want to point out that it is possible to couple the EM-WaveHoltz method to other type time-domain solvers such as spectral element method and continuous finite element method. Further, although we don't consider it here, our approach directly generalizes to linear dispersive frequency-domain models such as the generalized dispersive materials modeled through an auxiliary differential equation approach in [28].

A. Yee-EM-WaveHoltz

The Yee scheme [24], [25] or the finite-difference-time-domain (FDTD) method, is one of the most popular and successful methods in computational electromagnetics and can be easily turned into a fast FDFD method, the Yee-EM-WaveHoltz method, as follows.

Assume a uniform time step size $\Delta t = T/M$ and denote any given function at a point $(i\Delta x, j\Delta y, k\Delta z, n\Delta t)$ in (3+1) dimensions by

$$F_{i,j,k}^n = F(i\Delta x, j\Delta y, k\Delta z, n\Delta t). \quad (22)$$

Also denote any point in time $n\Delta t = t^n$. Then the Yee scheme to solve the time-domain problem in the EM-WaveHoltz formulation is

$$\begin{aligned} & \frac{(\tilde{H}_x)_{i,j+\frac{1}{2},k+\frac{1}{2}}^{n+\frac{1}{2}} - (\tilde{H}_x)_{i,j+\frac{1}{2},k+\frac{1}{2}}^{n-\frac{1}{2}}}{\Delta t} \\ &= \frac{1}{\mu_{i,j+\frac{1}{2},k+\frac{1}{2}}} \left(\frac{(\tilde{E}_y)_{i,j+\frac{1}{2},k+1}^n - (\tilde{E}_y)_{i,j+\frac{1}{2},k}^n}{\Delta z} \right. \\ & \quad \left. - \frac{(\tilde{E}_z)_{i,j+1,k+\frac{1}{2}}^n - (\tilde{E}_z)_{i,j,k+\frac{1}{2}}^n}{\Delta y} \right), \end{aligned} \quad (23a)$$

$$\begin{aligned} & \frac{(\tilde{H}_y)_{i+\frac{1}{2},j,k+\frac{1}{2}}^{n+\frac{1}{2}} - (\tilde{H}_y)_{i+\frac{1}{2},j,k+\frac{1}{2}}^{n-\frac{1}{2}}}{\Delta t} \\ &= \frac{1}{\mu_{i+\frac{1}{2},j,k+\frac{1}{2}}} \left(\frac{(\tilde{E}_z)_{i+1,j,k+\frac{1}{2}}^n - (\tilde{E}_z)_{i,j,k+\frac{1}{2}}^n}{\Delta x} \right. \\ & \quad \left. - \frac{(\tilde{E}_x)_{i+\frac{1}{2},j,k+1}^n - (\tilde{E}_x)_{i+\frac{1}{2},j,k}^n}{\Delta z} \right). \end{aligned} \quad (23b)$$

$$\begin{aligned} & \frac{(\tilde{H}_z)_{i+\frac{1}{2},j+\frac{1}{2},k}^{n+\frac{1}{2}} - (\tilde{H}_z)_{i+\frac{1}{2},j+\frac{1}{2},k}^{n-\frac{1}{2}}}{\Delta t} \\ &= \frac{1}{\mu_{i+\frac{1}{2},j+\frac{1}{2},k}} \left(\frac{(\tilde{E}_x)_{i+\frac{1}{2},j+1,k}^n - (\tilde{E}_x)_{i+\frac{1}{2},j,k}^n}{\Delta y} \right. \\ & \quad \left. - \frac{(\tilde{E}_y)_{i+1,j+\frac{1}{2},k}^n - (\tilde{E}_y)_{i,j+\frac{1}{2},k}^n}{\Delta x} \right), \end{aligned} \quad (23c)$$

and

$$\begin{aligned} & \epsilon_{i+\frac{1}{2},j,k} \frac{(\tilde{E}_x)_{i+\frac{1}{2},j,k}^{n+1} - (\tilde{E}_x)_{i+\frac{1}{2},j,k}^n}{\Delta t} = -\sin(\omega t^{n+\frac{1}{2}})(J_x)_{i+\frac{1}{2},j,k} \\ & + \left(\frac{(\tilde{H}_z)_{i+\frac{1}{2},j+\frac{1}{2},k}^{n+\frac{1}{2}} - (\tilde{H}_z)_{i+\frac{1}{2},j-\frac{1}{2},k}^{n+\frac{1}{2}}}{\Delta y} \right. \\ & \quad \left. - \frac{(\tilde{H}_y)_{i+\frac{1}{2},j,k+\frac{1}{2}}^{n+\frac{1}{2}} - (\tilde{H}_y)_{i+\frac{1}{2},j,k-\frac{1}{2}}^{n+\frac{1}{2}}}{\Delta z} \right), \end{aligned} \quad (24a)$$

$$\begin{aligned} & \epsilon_{i,j+\frac{1}{2},k} \frac{(\tilde{E}_y)_{i,j+\frac{1}{2},k}^{n+1} - (\tilde{E}_y)_{i,j+\frac{1}{2},k}^n}{\Delta t} = -\sin(\omega t^{n+\frac{1}{2}})(J_y)_{i,j+\frac{1}{2},k} \\ & + \left(\frac{(\tilde{H}_x)_{i,j+\frac{1}{2},k+\frac{1}{2}}^{n+\frac{1}{2}} - (\tilde{H}_x)_{i,j+\frac{1}{2},k-\frac{1}{2}}^{n+\frac{1}{2}}}{\Delta z} \right. \\ & \quad \left. - \frac{(\tilde{H}_z)_{i+\frac{1}{2},j,k+\frac{1}{2}}^{n+\frac{1}{2}} - (\tilde{H}_z)_{i-\frac{1}{2},j,k+\frac{1}{2}}^{n+\frac{1}{2}}}{\Delta x} \right), \end{aligned} \quad (24b)$$

$$\begin{aligned} & \epsilon_{i,j,k+\frac{1}{2}} \frac{(\tilde{E}_z)_{i,j,k+\frac{1}{2}}^{n+1} - (\tilde{E}_z)_{i,j,k+\frac{1}{2}}^n}{\Delta t} = -\sin(\omega t^{n+\frac{1}{2}})(J_z)_{i,j,k+\frac{1}{2}} \\ & + \left(\frac{(\tilde{H}_y)_{i+\frac{1}{2},j,k+\frac{1}{2}}^{n+\frac{1}{2}} - (\tilde{H}_y)_{i-\frac{1}{2},j,k+\frac{1}{2}}^{n+\frac{1}{2}}}{\Delta x} \right. \\ & \quad \left. - \frac{(\tilde{H}_x)_{i,j+\frac{1}{2},k+\frac{1}{2}}^{n+\frac{1}{2}} - (\tilde{H}_x)_{i,j-\frac{1}{2},k+\frac{1}{2}}^{n+\frac{1}{2}}}{\Delta y} \right). \end{aligned} \quad (24c)$$

For the initial step $\tilde{H}_x^{-\frac{1}{2}}$ is initialized as

$$\begin{aligned} & (\tilde{H}_x)_{i,j+\frac{1}{2},k+\frac{1}{2}}^{-\frac{1}{2}} = (\tilde{H}_x)_{i,j+\frac{1}{2},k+\frac{1}{2}}^0 \\ & - \frac{\Delta t}{2\mu_{i,j+\frac{1}{2},k+\frac{1}{2}}} \left(\frac{(\tilde{E}_y)_{i,j+\frac{1}{2},k+1}^0 - (\tilde{E}_y)_{i,j+\frac{1}{2},k}^0}{\Delta z} \right. \\ & \quad \left. - \frac{(\tilde{E}_z)_{i,j+1,k+\frac{1}{2}}^0 - (\tilde{E}_z)_{i,j,k+\frac{1}{2}}^0}{\Delta y} \right), \end{aligned} \quad (25)$$

and $\tilde{H}_y^{-\frac{1}{2}}$ and $\tilde{H}_z^{-\frac{1}{2}}$ are initialized similarly.

To approximate the filter operator Π in (26) we use the composite trapezoidal rule

$$\Pi_h \begin{pmatrix} \nu_E \\ \nu_H \end{pmatrix} = \frac{2\Delta t}{T} \sum_{n=0}^M \eta_n \left(\cos(\omega t^n) - \frac{1}{4} \right) \begin{pmatrix} \tilde{\mathbf{E}}^n \\ \tilde{\mathbf{H}}^{n+\frac{1}{2}} + \tilde{\mathbf{H}}^{n-\frac{1}{2}} \end{pmatrix}, \quad (26)$$

where

$$\eta_n = \begin{cases} \frac{1}{2}, & n = 0 \text{ or } M, \\ 1, & \text{otherwise.} \end{cases} \quad (27)$$

The solution obtained by the above iteration introduces an additional error from the time marching and as a result converges to a frequency-domain solution with a slightly perturbed frequency $\tilde{\omega}$, where $|\tilde{\omega} - \omega| = O(\Delta t^2)$. Of course since $\Delta t \sim \min\{\Delta x, \Delta y, \Delta z\}$ the EM-WaveHoltz solution is converging at the same rate as the spatial discretization but nevertheless it does have an additional error. This error is easily eliminated by a small modification which we discuss next.

B. Eliminating the temporal error in EM-WaveHoltz

For brevity we consider the energy conserving two dimensional TM model. Then $E_x = E_y = H_z = 0$ and we can neglect the k component. The Yee scheme for the corresponding time-domain equation is defined as:

$$\begin{aligned} & \epsilon_{i,j} \frac{(\tilde{E}_z)_{i,j}^{n+1} - (\tilde{E}_z)_{i,j}^n}{\Delta t} = \left(\frac{(\tilde{H}_y)_{i+\frac{1}{2},j}^{n+\frac{1}{2}} - (\tilde{H}_y)_{i-\frac{1}{2},j}^{n+\frac{1}{2}}}{\Delta x} \right. \\ & \quad \left. - \frac{(\tilde{H}_x)_{i,j+\frac{1}{2}}^{n+\frac{1}{2}} - (\tilde{H}_x)_{i,j-\frac{1}{2}}^{n+\frac{1}{2}}}{\Delta y} \right) - S^{n+\frac{1}{2}}(J_z)_{i,j} \end{aligned} \quad (28)$$

and

$$\frac{(\tilde{H}_x)_{i,j+\frac{1}{2}}^{n+\frac{1}{2}} - (\tilde{H}_x)_{i,j+\frac{1}{2}}^{n-\frac{1}{2}}}{\Delta t} = -\frac{1}{\mu_{i,j+\frac{1}{2}}} \frac{(\tilde{E}_z)_{i,j+1}^n - (\tilde{E}_z)_{i,j}^n}{\Delta y}, \quad (29a)$$

$$\frac{(\tilde{H}_y)_{i+\frac{1}{2},j}^{n+\frac{1}{2}} - (\tilde{H}_y)_{i+\frac{1}{2},j}^{n-\frac{1}{2}}}{\Delta t} = \frac{1}{\mu_{i+\frac{1}{2},j}} \frac{(\tilde{E}_z)_{i+1,j}^n - (\tilde{E}_z)_{i,j}^n}{\Delta x}, \quad (29b)$$

with initial conditions $E_z^0 = \nu$ and $H_x^0 = H_y^0 = 0$. $H_x^{-\frac{1}{2}}$ and $H_y^{-\frac{1}{2}}$ are initialized similar to (25). Here, the slight modification is that we use the second order accurate approximation

$$S^{\frac{1}{2}} = \frac{\omega \Delta t}{2}, \quad S^{n+\frac{1}{2}} = S^{n-\frac{1}{2}} + \Delta t \omega \cos(\omega t^n), \quad (30)$$

to $\sin(\omega t^{n+\frac{1}{2}})$. Using $S^{n+\frac{1}{2}}$ instead of $\sin(\omega t^{n+\frac{1}{2}})$ gives us a chance to eliminate the error due to the time discretization.

Eliminating H_x and H_y in (28) and (29), we have

$$\begin{aligned} & \frac{(\tilde{E}_z)_{i,j}^{n+1} - 2(\tilde{E}_z)_{i,j}^n + (\tilde{E}_z)_{i,j}^{n-1}}{\Delta t^2} + L_h(\tilde{E}_z)_{i,j}^n \\ &= -\left(\frac{1}{\epsilon_{i,j}} J_z\right)_{i,j} \frac{S^{n+\frac{1}{2}} - S^{n-\frac{1}{2}}}{\Delta t} \\ &= -\left(\frac{1}{\epsilon_{i,j}} J_z\right)_{i,j} \cos(\omega t^n), \end{aligned} \quad (31)$$

where

$$\begin{aligned} -L_h F_{i,j} &= \frac{1}{\epsilon_{i,j} \Delta x} \left(\frac{F_{i+1,j} - F_{i,j}}{\mu_{i+\frac{1}{2},j} \Delta x} - \frac{F_{i,j} - F_{i-1,j}}{\mu_{i-\frac{1}{2},j} \Delta x} \right) \\ &+ \frac{1}{\epsilon_{i,j} \Delta y} \left(\frac{F_{i,j+1} - F_{i,j}}{\mu_{i,j+\frac{1}{2}} \Delta y} - \frac{F_{i,j} - F_{i,j-1}}{\mu_{i,j-\frac{1}{2}} \Delta y} \right). \end{aligned} \quad (32)$$

(31) is an approximation to the second order form of the time-domain equation in EM-WaveHoltz. We now have the following theorem guaranteeing the convergence of the discrete iteration (for the energy conserving case)

Theorem 1. Let ν^∞ be the solution to

$$\tilde{\omega}^2 \nu^\infty - L_h \nu^\infty = \omega \left(\frac{1}{\epsilon} J \right), \quad \tilde{\omega} = \frac{\sin(\omega \Delta t / 2)}{\Delta t / 2}. \quad (33)$$

Further, let $\{-\lambda_j^2\}_{j=1}^N$ and $\{\psi_j\}_{j=1}^N$ be the eigenvalues and corresponding eigenfunctions of L_h , and $0 < \lambda_1 < \lambda_2 < \dots < \lambda_N$. Assume that ω is not a resonance and denote the relative distance to the closest resonance $\delta_h = \min_j |\lambda_j - \omega| / \omega > 0$.

Then, for the energy conserving method, (28) - (29), with the filter (26), the Yee-EM-WaveHoltz iteration $\nu^{(k+1)} = \Pi_h \nu^{(k)}$ with $\nu^{(0)} = 0$ converges to ν^∞ as long as

$$\Delta t \leq \frac{2}{\lambda_N + 2\omega/\pi}, \quad \omega \Delta t \leq \min(\delta_h, 1). \quad (34)$$

Moreover, the convergence rate is at least $\rho_h = \max(1 - 0.3\delta_h^2, 0.6)$.

The proof of this Theorem is presented in Appendix C.

We note that the first constraint on the timestep is essentially the standard CFL condition for an explicit method while the

second condition could be very strict. In actual computations we never observe that violation of the second condition leads to problems and conjecture that it is likely a mathematical artifact rather than a practical limitation.

Now, if we replace $\cos(\omega t^n)$ with $\cos(\tilde{\omega} t^n)$ in (30) with

$$\tilde{\omega} = \frac{2}{\Delta t} \sin^{-1} \left(\frac{\omega \Delta t}{2} \right), \quad (35)$$

and modify the trapezoidal weights in the filter as

$$\hat{\Pi}_h \nu = \frac{2\Delta t}{T} \sum_{n=0}^M \left(\cos(\omega t^n) - \frac{1}{4} \right) \frac{\cos(\omega t^n)}{\cos(\tilde{\omega} t^n)} \tilde{E}_z^n. \quad (36)$$

Then Theorem 1 holds but the convergence is to ν^∞ being the solution to the standard discretized frequency-domain problem

$$\omega^2 \nu^\infty - L_h \nu^\infty = \omega \left(\frac{1}{\epsilon} J \right). \quad (37)$$

The derivation of this strategy is discussed in Appendix D along with the proof of Theorem 1.

C. DG-EM-WaveHoltz

The discontinuous Galerkin (DG) method, due to its high order accuracy, flexibility to use nonconforming meshes and its suitability for parallel implementation, has become increasingly popular for the simulation of time-domain wave propagation. As for the Yee scheme, DGTD can easily be turned into a frequency-domain solver using our approach. Here we use the time-domain DG method of [3], [26].

Consider Maxwell's equation in d -dimensions. Let Ω_j be an element, and $P^s(\Omega_j)$ be the space of polynomials at most degree s . Define $V_h^s(\Omega_j) = (P^s(\Omega_j))^d$ to be the corresponding vector polynomial space. The DG method seeks the solution $\mathbf{E}_h \in V_h^s(\Omega_j)$, $\tilde{\mathbf{H}}_h \in V_h^s(\Omega_j)$ such that for any $\phi \in V_h^s(\Omega_j)$, $\psi \in V_h^s(\Omega_j)$

$$\begin{aligned} \int_{\Omega_j} \partial_t \tilde{\mathbf{E}}_h \cdot \phi d\mathbf{V} &= \int_{\Omega_j} \tilde{\mathbf{H}}_h \cdot \nabla \times \left(\frac{1}{\epsilon} \phi \right) d\mathbf{V} \\ &+ \int_{\partial\Omega_j} (\hat{\mathbf{H}} \times \mathbf{n}) \cdot \left(\frac{1}{\epsilon} \phi \right) ds - \int_{\Omega_j} \sin(\omega t) \mathbf{J} \cdot \phi d\mathbf{V}, \end{aligned} \quad (38a)$$

$$\begin{aligned} \int_{\Omega_j} \partial_t \tilde{\mathbf{H}}_h \cdot \psi d\mathbf{V} &= - \int_{\Omega_j} \tilde{\mathbf{E}}_h \cdot \nabla \times \left(\frac{1}{\mu} \psi \right) d\mathbf{V} \\ &- \int_{\partial\Omega_j} (\hat{\mathbf{E}} \times \mathbf{n}) \cdot \left(\frac{1}{\mu} \psi \right) ds. \end{aligned} \quad (38b)$$

Here, \mathbf{n} is the outward pointing normal of a face and $\hat{\mathbf{H}}$ and $\hat{\mathbf{E}}$ are numerical fluxes. A stable and accurate choice for the numerical fluxes is

$$\hat{\mathbf{H}} = \{\tilde{\mathbf{H}}\} + \alpha[\tilde{\mathbf{E}}], \quad \hat{\mathbf{E}} = \{\tilde{\mathbf{E}}\} + \beta[\tilde{\mathbf{H}}]. \quad (39)$$

Here \mathbf{v}^\pm denotes the two values on each side of a face, $\{\mathbf{v}\} = \frac{1}{2}(\mathbf{v}^+ + \mathbf{v}^-)$ is the average and $[\mathbf{v}] = \mathbf{n}^+ \times \mathbf{v}^+ + \mathbf{n}^- \times \mathbf{v}^-$ is the jump. The semi-discretization (38) can be evolved in a method of lines fashion, using for example a Runge-Kutta method as the time stepper. Depending on the time discretization it may be possible to eliminate the time error as discussed above but we don't pursue this here. Further, in the examples below we always use the trapezoidal rule to discretize the filter.

III. NUMERICAL RESULTS

In this section we demonstrate the performance of the EM-WaveHoltz methods on several examples in two and three dimensions. The sin-forcing formulation is used in two dimensions and the cos-forcing formulation is used in three dimensions, unless otherwise specified.

A. Accuracy test in two dimensions with Yee-EM-WaveHoltz

As a first test we solve the 2D TM model. We non-dimensionalize the equations so that $\epsilon = \mu = 1$ and manufacture a forcing such that the exact solution is $E_z(x, y) = 16x^2(x-1)^2y^2(y-1)^2$. This solution is compatible with perfect electric conductor (PEC) boundary conditions on the domain $[0, 1]^2$. We apply the Yee scheme and the EM-WaveHoltz iteration with GMRES acceleration.

To test the convergence for a) one frequency in one solve, and b) multiple frequencies in one solve, we perform a grid refinement study at fixed frequencies $\omega_1 = 5.5$, $3\omega_1$ and $7\omega_1$. In Figure 1, we display how the error is decreased as the grid size is reduced. As expected, for both of one frequency in one solve and multiple frequencies in one solve, we observe second order convergence. However, there is a difference in the amplitude of the error between the solutions obtained using the two approaches. For the same frequency, one frequency in one solve is more accurate than multiple frequencies in one solve.

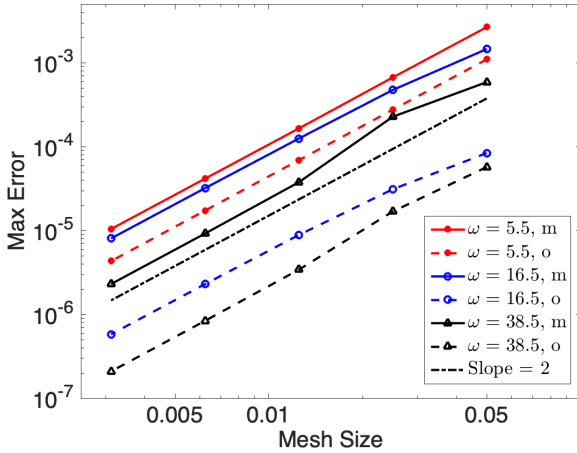


Fig. 1. Grid convergence of a manufactured solution. Here “o” stands for one frequency in one solve, and “m” stands for multiple frequencies in one solve. The errors displayed are for E_z for a 2D TM model.

B. Eliminating the temporal error in Yee-EM-WaveHoltz

Again, let $\epsilon = \mu = 1$ and consider the 2D TM model on the domain $[0, 1]^2$. We choose the forcing and the non-zero Dirichlet boundary conditions so that the exact solution is $E_z(x, y) = x + y$. As this is a polynomial with total degree one, the spatial part of the Yee scheme is exact and we should be able to fully eliminate all errors by using the modified quadrature designed to eliminate the temporal error. To recap, in the modification we apply $S^{n+\frac{1}{2}}$ in (30) with the

frequency modification (35) to approximate $\sin(\omega t^{n+\frac{1}{2}})$ and use the modified numerical quadrature (36).

To confirm that the temporal error is eliminated we compute solutions for the frequencies $\omega = 10.5, 20.5, 30.5, 40.5, 50.5$ on a grid with 20 gridpoints in each direction using the GMRES accelerated Yee-EM-WaveHoltz iteration.

TABLE I

CONFIRMATION OF THE ELIMINATION OF THE TEMPORAL ERRORS FOR THE YEE-EM-WAVEHOLTZ METHOD WHEN THE MODIFIED QUADRATURE IS USED. THE ERRORS ARE FOR E_z AND FOR DIFFERENT FREQUENCIES.

ω	10.5	20.5	30.5	40.5	50.5
Error	1.03E-13	4.65E-13	4.43E-13	6.07E-13	3.83E-13

The results, presented in Table I, show that the modified quadrature does eliminate the temporal errors.

C. Number of iterations for different frequencies and boundary conditions in two dimensions

In this experiment we solve the 2D TM model with the source

$$J_z = -\omega \exp(-\sigma((x-0.01)^2 + (y-0.015)^2)), \quad (40)$$

where $\sigma = \max(36, \omega^2)$, $\epsilon = \mu = 1$, and the computational domain is $[-1, 1]^2$. Here we sweep over the frequencies $\omega = k + \frac{1}{2}$, $1 \leq k \leq 100$. We use the GMRES accelerated Yee-EM-WaveHoltz iteration and to keep the solution reasonably well resolved we use $8\lceil\omega\rceil$ grids in each directions.

We solve this problem with 6 different boundary conditions: (1) 4 open boundaries, (2) 1 PEC boundary and 3 open boundaries, (3) 2 parallel PEC boundaries and 2 open boundaries, (4) 2 PEC boundaries next to each other forming a PEC corner and 2 open boundaries, (5) 3 PEC boundaries and 1 open boundary, (6) 4 PEC boundaries. The rationale here is that in problems (1), (2) and (4) there will not be any opposing PEC walls where waves can be “trapped” while in the other three problems there are.

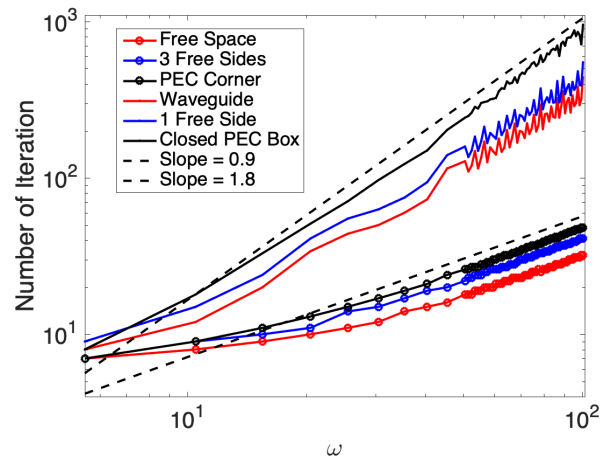


Fig. 2. Number of iterations as a function of frequency for the six different 2D TM problems.

We also note that in the open directions we employ the optimally accurate double absorbing boundary layer (DAB) by

Hagstrom et al. [29]. The order of approximation in the DAB layers we use is 10 which virtually makes the non-reflecting boundary conditions exact.

In the EM-WaveHoltz iteration, we use 10 periods so that $T = 10 \frac{2\pi}{\omega}$. This reduces the memory consumption in GMRES by a factor 10 and reduces the number of iterations by nearly a factor of 10 (the cost per iteration of course goes up by 10 as well). In Fig. 2, the number of iteration required to reduce the relative residual below 10^{-7} are presented. We observe that for the problems without trapped waves, the number of iterations scales approximately as $\omega^{0.9}$. For the problems with trapped waves, the iteration converges slower and the number of iterations scales as approximately $\omega^{1.8}$.

D. Number of iterations for different frequencies and boundary conditions in three dimensions

In this example we solve the 3D Maxwell's equation with a source

$$J_x = -\omega \exp(-\sigma(x^2 + y^2 + z^2)), J_y = J_z = 0. \quad (41)$$

Here $\sigma = \max(36, \omega^2)$, $\epsilon = \mu = 1$ and the computational domain is $[-1, 1]^3$.

To measure how the number of iterations grow with the frequency, three different problems are considered: (1) an open domain, (2) two parallel PEC plates, (3) five PEC boundaries and one free side on the most left side. Again, we still apply the highly accurate double absorbing boundary layer (DAB) for non-reflecting boundary conditions. The order of the DAB layers is set as 5 guaranteeing that the error of the non-reflecting boundary conditions is well below the discretization error.

We sweep over frequencies and use the GMRES accelerated Yee-EM-WaveHoltz method with the cos-forcing. To have a well resolved solution we use $4\lceil\omega\rceil$ elements in each direction. In the EM-WaveHoltz iteration, we set T as 5 periods.

In Figure 3, iteration numbers to reduce the relative residual below 10^{-6} are presented. The total number of iterations is estimated to scale as $\omega^{0.9}$ for the open problem, $\omega^{1.9}$ for the parallel PEC plate problem and $\omega^{2.5}$ for the problem with one free side.

We also use the the sin-forcing to simulate the open domain problem with the same mesh and the error tolerance. We observe that the number of iteration is exactly the same as the cos-forcing, though the relative residual is slightly different for high frequencies.

E. Smaller Krylov subspaces by longer filter time

As we mentioned before, we can filter over multiple periods $T = N \frac{2\pi}{\omega}$, which allows the further propagation of the wave. We consider $T = N \frac{2\pi}{\omega}$ with $N = 1, 3, 5$ for 2D and 3D open domain problem. The setup of this test is the same as Section III-C for 2D and Section III-D for 3D. We scan over different frequencies and apply the GMRES accelerated Yee-EM-WaveHoltz. The total number of iteration allowed is set as 200 in 2D and 100 in 3D. As can be seen in Figure 4 for high frequencies both the 2D and the 3D solver, when

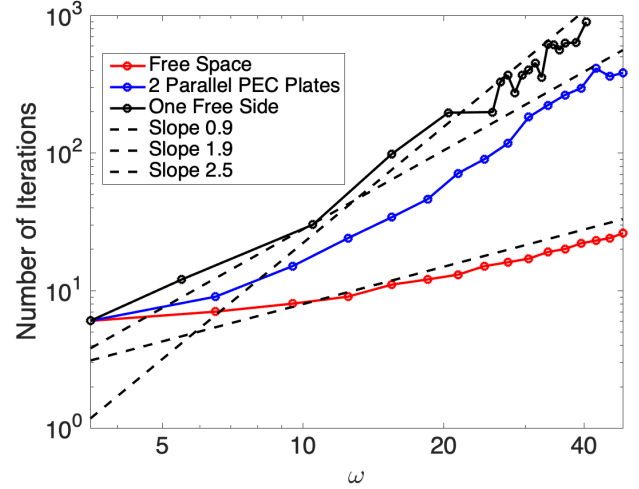


Fig. 3. Number of iterations as a function of frequency for different 3D problems.

using $T = \frac{2\pi}{\omega}$, fails to converge to the desired tolerance before reaching the maximum number of iterations.

In Figure 4, we present unscaled number of iterations against the frequency and observe that the number of iterations decays as the propagation time T in the time-domain grows. To further quantify the relation between the computational cost and $T = N \frac{2\pi}{\omega}$, we scale the number of iterations by N and present the result in Figure 5. We observe that for $N = 3$ and 5 the scaled curves collapse, implying that the total computational time is approximately the same. Thus, without increasing the computational cost, filtering over longer time can decrease the number of iterations, which in turn reduces the size of the Krylov subspace used by GMRES.

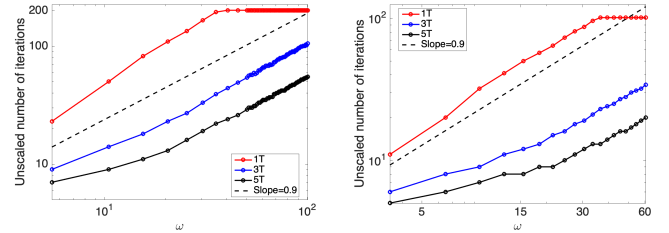


Fig. 4. Unscaled number of iterations as a function of frequency for different filtering time. Top: 2D open problem. Bottom: 3D open problem.

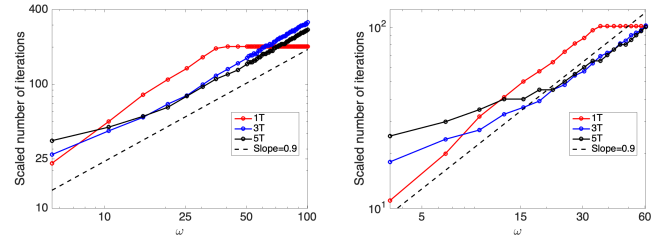


Fig. 5. Scaled number of iterations = $N \times$ number of iterations, if $T = N \frac{2\pi}{\omega}$. Scaled number of iterations as a function of frequency for different filtering time. Top: 2D open problem. Bottom: 3D open problem.

F. Number of iterations for different points per wavelength

TABLE II
NUMBER OF ITERATIONS FOR DIFFERENT NUMBER OF POINTS PER WAVELENGTH, 2D-TM MODEL

Boundaries	N	$2\lceil\omega\rceil$	$4\lceil\omega\rceil$	$6\lceil\omega\rceil$	$8\lceil\omega\rceil$
open	$\omega = 12.5$	9	9	9	9
PEC	$\omega = 12.5$	11	11	11	11
open	$\omega = 25.5$	13	12	12	12
PEC	$\omega = 25.5$	25	24	24	24

Here, we fix the frequency and investigate the number of iterations needed for convergence for different number of grid points per wavelength. We use the Yee-EM-WaveHoltz method with GMRES acceleration, and $\epsilon = \mu = 1$ is considered. For the 2D-TM model, we consider the computational domain $[-1, 1]^2$ and the source

$$J_z = \omega \exp(-144(x^2 + y^2)), \quad (42)$$

with either 4 open boundaries or 4 PEC boundaries. For the 3D model, we consider the computational domain $[-1, 1]^3$ and the source

$$J_x = -\omega \exp(-144(x^2 + y^2 + z^2)), \quad J_y = J_z = 0, \quad (43)$$

with either 6 open boundaries or 6 PEC boundaries. In each direction, we use N grid points. We take $T = 10\frac{2\pi}{\omega}$. The stopping criteria is that the relative residual falls below 10^{-8} for the 2D TM-model and 10^{-5} for the 3D model.

The results are presented in Table II and Table III. When considering an open problem at a fixed frequency, we observe that the number of iterations does not change as the number of grid points per wavelength is increased. For the PEC problem in three dimensions the number of iterations are reduced slightly as the resolution is increased and for the 2D PEC problem it does not change significantly. Based on this experiment and other experiments (not reported) our observation is that the algorithm is robust with respect to resolution (but of course the discretization error will depend on the resolution.)

TABLE III
NUMBER OF ITERATIONS FOR DIFFERENT NUMBER OF POINTS PER WAVELENGTH, 3D.

Boundaries	N	$2\lceil\omega\rceil$	$4\lceil\omega\rceil$	$6\lceil\omega\rceil$	$8\lceil\omega\rceil$
open	$\omega = 12.5$	5	5	5	6
PEC	$\omega = 12.5$	26	24	23	22
open	$\omega = 25.5$	7	7	7	7
PEC	$\omega = 25.5$	174	153	150	135

G. Verification of the SPD structure for energy conserving 2D TM-model

Here, we consider the 2D TM model with PEC boundary conditions, $\epsilon = \mu = 1$ and the Gaussian source

$$J_z = -\omega \exp(-\omega^2(x^2 + y^2)), \quad (44)$$

on the computational domain $[-1, 1]^2$. We apply the Yee-EM-WaveHoltz method, and we use this example to verify

that our method results in a SPD linear system. The code is implemented in a matrix free manner. The matrix $I - S$ is constructed column by column through the calculation of matrix-vector multiplication $(I - S)e_i$ where e_i is a column vector whose i -th element is 1 and all other elements are 0.

We first compare $I - S$ and $(I - S)^T$. The L_∞ norm of their difference is always on the level of machine accuracy. The eigenvalues of the matrix for $\omega = 25$ with $N = 100$, $N = 125$ grid points in each direction are presented in Figure 6. We observe that all the eigenvalues are positive. The condition number of $I - S$ is approximately 3.16×10^4 for $N = 100$ and 7.36×10^5 for $N = 125$.

We use CG method and GMRES method in the Yee-EM-WaveHoltz method for the above example with $\omega = 25$ and $N = 100$ grid points in each direction. The convergence history for both methods are presented in Figure 6. The total iteration number needed for convergence of these two methods are comparable for this example.

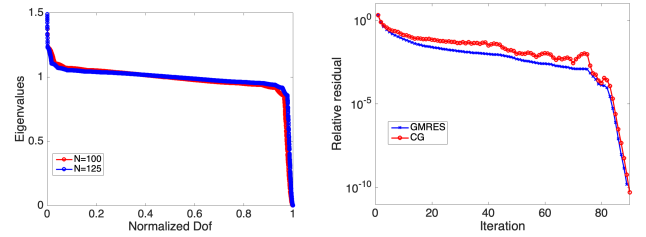


Fig. 6. Left: Eigenvalues of $I - S$ for Yee-EM-WaveHoltz and $\omega = 25$ with N grid points in each direction. For the i -th eigenvalue, normalized DOF = i divided by total number of degrees of freedom. Right: Convergence history of the CG method and the GMRES method with Yee-EM-WaveHoltz, $\omega = 25$ and $N = 100$ grid points in each direction.

H. Simulation of an optical nano slit

Nano optical slits have wide applications in plasmonics and metamaterials, for example [30], [31], [32]. We consider the 2D TM model and the PEC slit in Fig. 7. A line source is located at $y = -0.5\mu m$. We apply the Yee-EM-WaveHoltz with GMRES acceleration to simulate the propagation of the electromagnetic wave in this device. The wavelength is chosen as $\lambda = 0.25\mu m$. The numerical result is presented in Fig. 8. In the slit region, the electromagnetic wave propagates and interact with reflected wave. When the electromagnetic wave propagates and exits the slit, it is decoupled to radiation modes.

I. Simulation of a photonic crystal waveguide

Following [33] we also consider a photonic crystal waveguide depicted in Fig. 9. In the figure the black circles represent crystal cylinders and the white part represents vacuum. The relative permittivity of the crystal cylinders is 11.4. The distance between the center of the crystal cylinders is $a = 0.42\mu m$ and the radius of each photonic crystal is $r = 0.25a$. To drive the problem we place a point source in the center of the computational domain. The solution for the wavelength $\lambda = 1.44\mu m$ is presented in Fig. 10. It is clear that the design guides the E_z wave to propagate along the direction of the waveguide at this wavelength.

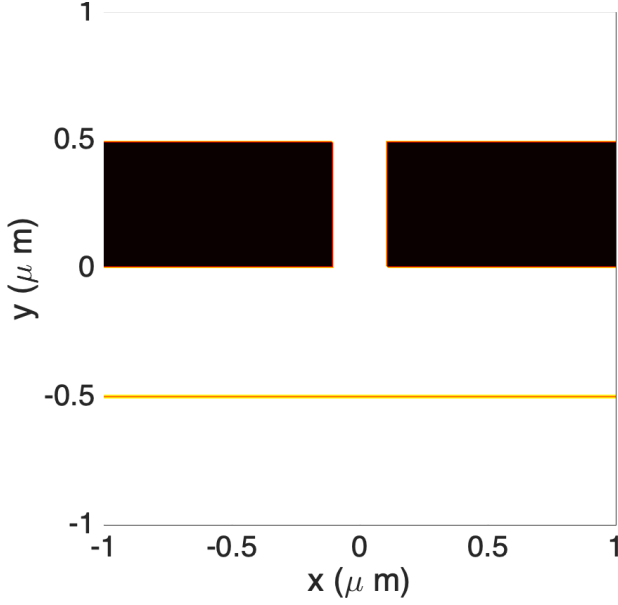


Fig. 7. Geometry of a PEC slit. White: vacuum. Black: PEC scatter. Yellow: line source.

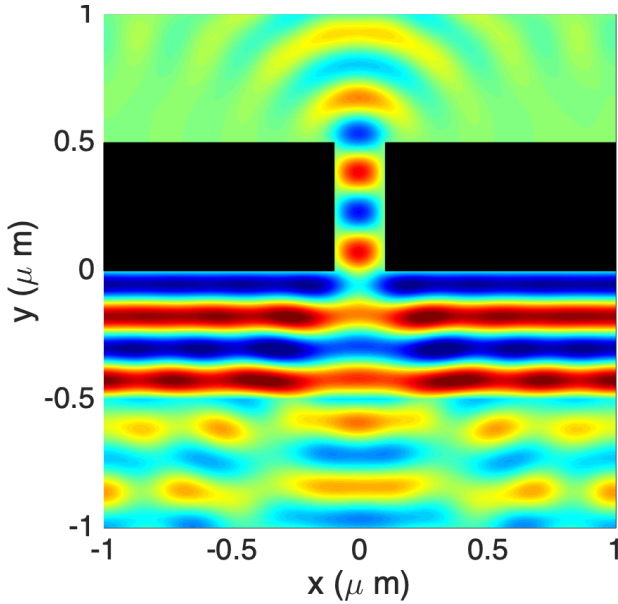


Fig. 8. Normalized E_z for the slit in Fig. 7 with $\lambda = 0.25\mu\text{m}$. Black: slit. Red:1. Blue:-1.

As the wavelength λ changes, the behavior of the electromagnetic wave propagation in this device varies. To study this behavior we sweep over many frequencies.

To measure the strength of the electric field in the channel of the waveguide, we define $S = \sqrt{\int_{-0.5a}^{0.5a} \int_{15.75a}^{21a} E_z^2 dx dy}$. We set S_{ref} as the S for the wavelength $\lambda = 1.44\mu\text{m}$. For certain λ , the wave mainly propagates along the direction of the waveguide, while the propagation along this direction may be limited for other wavelengths. The former corresponds to large values of S/S_{ref} while the latter corresponds to small values.

The ratio of S/S_{ref} as a function of the normalized wave-

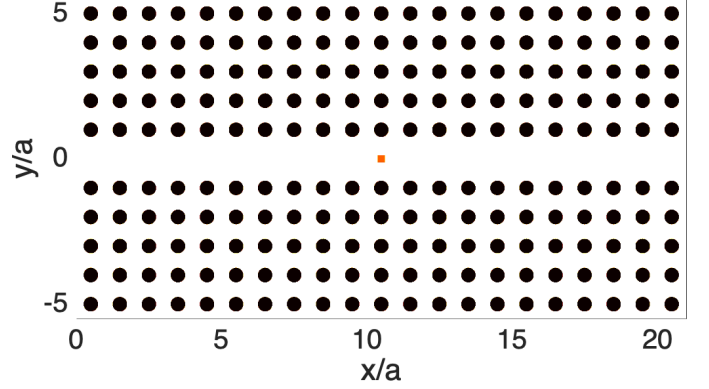


Fig. 9. Geometry of a photonic crystal waveguide. Here, $a = 0.42\mu\text{m}$. White: vacuum. Black: photonic crystal. Red: point source.

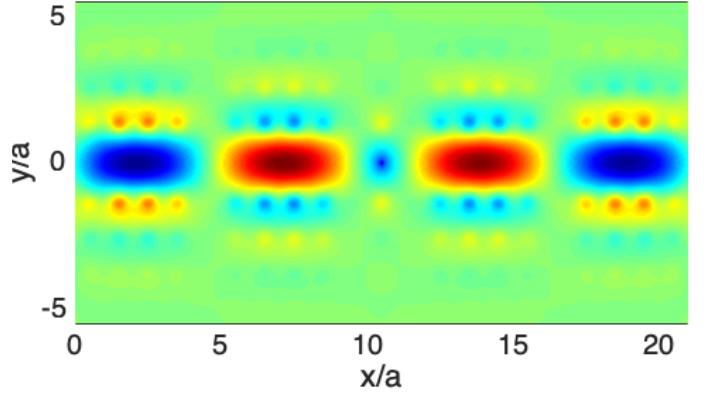


Fig. 10. Normalized E_z for the photonic crystal waveguide in Fig. 10 with $a = 0.42\mu\text{m}$ and the wavelength $\lambda = 1.44\mu\text{m}$. Red:1. Blue:-1.

length λ/a is reported in Fig. 11. We observe that, overall, from $\lambda = 3a$ to $\lambda = 3.5a$, S grows as λ increases. Then, from $\lambda = 3.5a$ to $\lambda = 3.9a$, S decays exponentially fast as the wavelength grows.

J. Multiple frequencies in one solve

Here, we follow the idea described in Section I-C and obtain solutions for multiple frequencies in one solve. We consider a photonic crystal device with similar set-up to that in Section III-I with the difference being that y ranges from $[-4.5a, 4.5a]$. We take the wavelength $\lambda = 3a, 1.5a, 0.75a$. We use the Yee-EM-WaveHoltz for this example. In Fig. 12, we compare the results of computing the solutions for different frequencies in one solve and one frequency in one solve with the same mesh. Visually, these two results match each other well. This confirms the effectiveness of our strategy to simulate multiple frequencies in one solve. We also observe that the iteration number and the computing time for multiple frequencies in one solve is close to the single frequency simulation for the highest frequency.

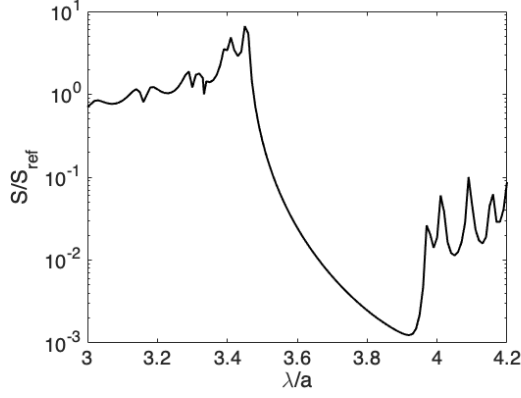


Fig. 11. Displayed is S as a function of the wavelength in the photonic crystal waveguide. Here, $a = 0.42\mu\text{m}$, and S_{ref} is obtained with the wavelength $\lambda = 1.44\mu\text{m}$.

K. DG-EM-WaveHoltz

Next we combine the EM-WaveHoltz iteration and the upwind nodal discontinuous Galerkin method [3]. We first solve the 2D TM model with $\epsilon = \mu = 1$, $J_z = \omega \exp(-144(x^2 + y^2))$ and $\omega = 12.5$ with PEC boundary conditions in the domain $[-1, 1]^2$. We use 4th order polynomials to represent the solution on each element and the classical Runge-Kutta time integrator of order 4.

We compare the results of the DG-EM-WaveHoltz and the Yee-EM-WaveHoltz. We use the unstructured mesh in Fig. 13 for the DG method and a 100×100 uniform mesh for the Yee scheme. The results obtained by these two methods are presented in Fig. 13. As can be seen they match each other well.

We also consider the 2D TM model with the same setup on a unit circle. We use the DG-EM-WaveHoltz with 7th order polynomial and the curvilinear mesh in Figure 14. The numerical result is presented in Figure 14. With a high order DG method, the EM-WaveHoltz obtains a reasonable numerical solution on a relatively coarse mesh for this curvilinear geometry.

IV. CONCLUSION

In this paper, we proposed the EM-WaveHoltz method, which converts the frequency-domain problem into a time-domain problem with time periodic forcing. The main advantages of the proposed method are as follows.

- 1) The resulting linear system is positive definite, and the GMRES iterative solver converges reasonably fast even though no preconditioning was used.
- 2) The method is flexible and straightforward to implement, it only requires a time-domain solver. In this paper, we illustrated how either the classical Yee scheme or a discontinuous Galerkin method can be used to construct frequency-domain solvers.
- 3) A unique feature of our EM-WaveHoltz method is that the solution to multiple frequencies can be obtained in a single solve.

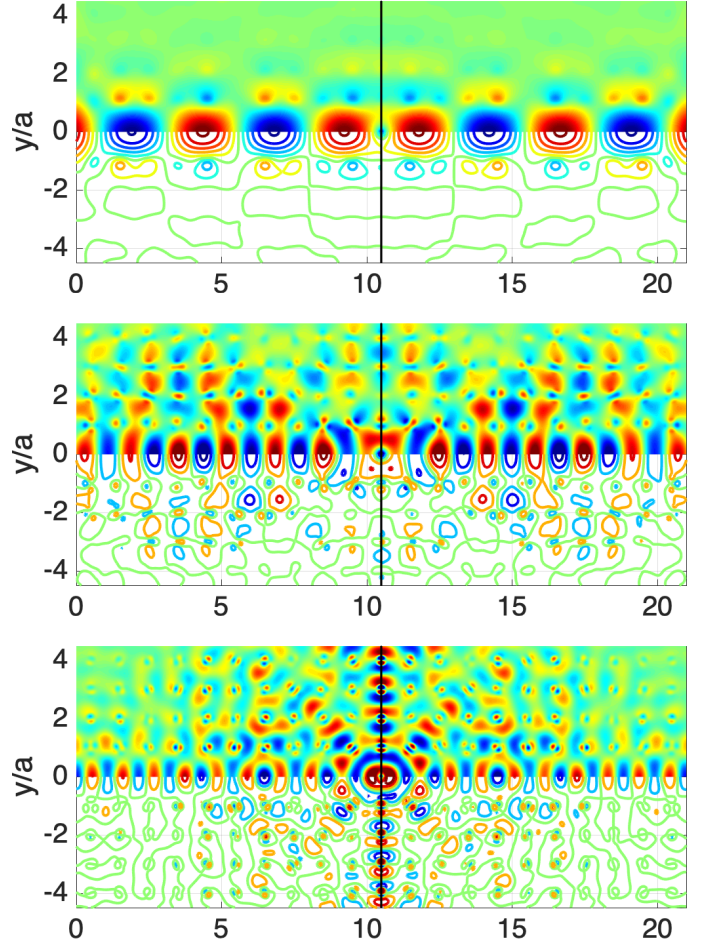


Fig. 12. Compare normalized E_z obtained by multiple frequencies in one solve and one frequency in one solve. Top to bottom, wavelengths $\lambda = 3a, 1.5a, 0.75a$. Left: Multiple frequencies in one solve. Right: One frequency in one solve.

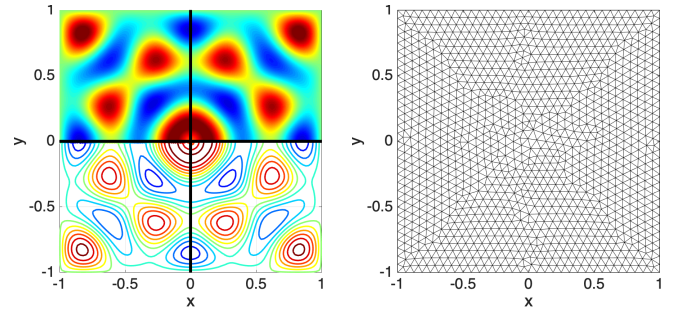


Fig. 13. Left figure: A comparison of E_z obtained by DG and Yee. Left part: DG. Right part: Yee. Blue: -0.4. Red: 0.4. Right figure: Unstructured mesh used for the DG method when comparing the DG-EM-WaveHoltz and the Yee-EM-WaveHoltz methods.

Potential future research directions are to design preconditioning strategies to further accelerate the convergence of the proposed iterative method. It would also be interesting to apply the method to more advanced dispersive material models.

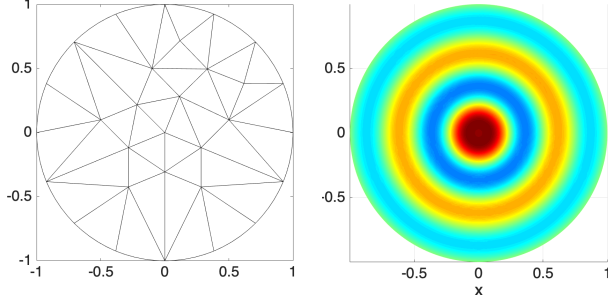


Fig. 14. Left: Curvilinear mesh for the unit circle. Right: DG solution for the Gaussian source on the unit circle with $\omega = 12.5$.

APPENDIX A

DERIVATION OF THE EM-WAVEHOLTZ ITERATION WITH COS-FORCING

The real valued $T = 2\pi/\omega$ -periodic solutions to (9) is in the form:

$$\tilde{\mathbf{E}} = \hat{\mathbf{E}}_0 \cos(\omega t) + \hat{\mathbf{E}}_1 \sin(\omega t), \quad (45)$$

$$\tilde{\mathbf{H}} = \hat{\mathbf{H}}_0 \cos(\omega t) + \hat{\mathbf{H}}_1 \sin(\omega t). \quad (46)$$

Matching the $\sin(\omega t)$ and $\cos(\omega t)$ term, we reach

$$\begin{aligned} \epsilon\omega(-\hat{\mathbf{E}}_0) &= \nabla \times \hat{\mathbf{H}}_1, \\ \epsilon\omega(\hat{\mathbf{E}}_1) &= \nabla \times \hat{\mathbf{H}}_0 - \mathbf{J}, \\ \mu\omega(-\hat{\mathbf{H}}_0) &= -\nabla \times \hat{\mathbf{E}}_1, \\ \mu\omega(\hat{\mathbf{H}}_1) &= -\nabla \times \hat{\mathbf{E}}_0. \end{aligned}$$

Based on (2), it follows that

$$\hat{\mathbf{E}}_0 = \Re\{\mathbf{E}\}, \quad \hat{\mathbf{H}}_0 = \Re\{\mathbf{H}\}, \quad \hat{\mathbf{E}}_1 = -\Im\{\mathbf{E}\}, \quad \hat{\mathbf{H}}_1 = -\Im\{\mathbf{H}\}.$$

By construction, one can further verify that $\Pi(\Im\{\mathbf{E}\}, \Im\{\mathbf{H}\})^T = (\Re\{\mathbf{E}\}, \Re\{\mathbf{H}\})^T$.

APPENDIX B

ANALYSIS OF ENERGY CONSERVING EM-WAVEHOLTZ ITERATION

Similar to [1], we analyze the convergence of the simplified EM-WaveHoltz iteration for the energy conserving case and show that $I - S$ is a self-adjoint positive definite operator.

Eliminating \mathbf{H} in the frequency-domain equation (1), we have

$$-\omega^2 \epsilon \mathbf{E} = -\nabla \times \left(\frac{1}{\mu} \nabla \times \mathbf{E} \right) - i\omega \mathbf{J}. \quad (47)$$

With the real-valued current source J , we further have

$$-\epsilon\omega^2 \Im(\mathbf{E}) = -\nabla \times \left(\frac{1}{\mu} \nabla \times \Im(\mathbf{E}) \right) - \omega \mathbf{J}. \quad (48)$$

Eliminating $\tilde{\mathbf{H}}$ in the time-domain equation (4), we obtain

$$\epsilon \partial_{tt} \tilde{\mathbf{E}} = \nabla \times \left(\frac{1}{\mu} \nabla \times \tilde{\mathbf{E}} \right) - \omega \cos(\omega t) \mathbf{J}, \quad (49)$$

with $\tilde{\mathbf{E}}|_{t=0} = \nu_E$ and $\tilde{\mathbf{E}}_t = \mathbf{0}$.

Suppose there is an orthonormal basis of $L^2(\Omega)$ consisted by the eigenfunctions of the operator $-\frac{1}{\epsilon} \nabla \times \left(\frac{1}{\mu} \nabla \times \right)$. Let

the eigenfunctions $\{\phi_j\}_{j=1}^\infty$ consist an orthonormal basis of the L^2 space. Let $\{-\lambda_j^2\}_{j=1}^\infty$ denote the corresponding nonpositive eigenvalues. For simplicity of notations, we let $\nu_E = \nu$. Then, $\mathbf{E}, \tilde{\mathbf{E}}, \mathbf{J}, \nu$ can be expanded as:

$$\begin{aligned} \mathbf{E} &= \sum_{j=1}^\infty \mathbf{E}_j \phi_j, \quad \tilde{\mathbf{E}} = \sum_{j=1}^\infty \tilde{\mathbf{E}}_j \phi_j, \\ \mathbf{J} &= \sum_{j=1}^\infty \mathbf{J}_j \phi_j, \quad \nu = \sum_{j=1}^\infty \nu_j \phi_j. \end{aligned} \quad (50)$$

Solve (47) and (49):

$$\mathbf{E}_j = \frac{\frac{1}{\epsilon} \omega \mathbf{J}_j}{\lambda_j^2 - \omega^2}, \quad (51)$$

$$\tilde{\mathbf{E}}_j = \mathbf{E}_j (\cos(\omega t) - \cos(\lambda_j t)) + \nu_j \cos(\lambda_j t). \quad (52)$$

Then,

$$\Pi \nu = \sum_{j=1}^\infty \bar{\nu}_j \phi_j, \quad \bar{\nu}_j = (1 - \beta(\lambda_j)) \mathbf{E}_j + \beta(\lambda_j) \nu_j, \quad (53)$$

where

$$\beta(\lambda) = \frac{2}{T} \int_0^T \left(\cos(\omega t) - \frac{1}{4} \right) \cos(\lambda t) dt. \quad (54)$$

Realizing that

$$\begin{aligned} \Pi \mathbf{0} &= \sum_{j=1}^\infty ((1 - \beta(\lambda_j)) \mathbf{E}_j + \beta(\lambda_j) \mathbf{0}) \\ &= \sum_{j=1}^\infty (1 - \beta(\lambda_j)) \mathbf{E}_j, \end{aligned} \quad (55)$$

we have

$$S \sum_{j=1}^\infty \nu_j \phi_j = \Pi \nu - \Pi \mathbf{0} = \sum_{j=1}^\infty \beta(\lambda_j) \nu_j \phi_j. \quad (56)$$

Furthermore, as proved in [1], the spectral radius ρ of S is strictly smaller than 1:

$$\rho \sim 1 - 6.33\delta^2, \quad \delta = \inf_j \frac{\lambda_j - \omega}{\omega}. \quad (57)$$

As a result, when ω is not a resonance,

$$\lim_{n \rightarrow \infty} (\Pi \nu^n - \mathbf{E}) = \lim_{n \rightarrow \infty} S^n (\nu^0 - \mathbf{E}) \rightarrow \mathbf{0}. \quad (58)$$

Furthermore,

$$((I - S)\nu, \nu) \geq (1 - \rho) \|\nu\|^2 > 0. \quad (59)$$

This also verifies that $I - S$ is positive definite. One can easily verify that $I - S$ is self-adjoint based on the expansion (56).

APPENDIX C

PROOF OF THEOREM 1

Proof of Theorem 1. Proof of Theorem 1 is similar to the proof of Theorem 2.4 of [1]. Here, we only point out the key steps. We expand all functions as

$$\begin{aligned}\tilde{E}_z^n &= \sum_{j=1}^N (\tilde{E}_z)_j^n \psi_j, \quad J_z = \sum_{j=1}^N (J_z)_j \psi_j, \\ (E_z) &= \sum_{j=1}^N (E_z)_j \psi_j, \quad \nu^\infty = \sum_{j=1}^N \nu_j^\infty \psi_j.\end{aligned}\quad (60)$$

Then,

$$(E_z)_j = \frac{\frac{1}{\epsilon} \omega (J_z)_j}{\omega^2 - \lambda_j^2}, \quad \nu_j^\infty = \frac{\frac{1}{\epsilon} \omega (J_z)_j}{\tilde{\omega}^2 - \lambda_j^2}. \quad (61)$$

Moreover, for $n \neq 0$

$$\begin{aligned}(\tilde{E}_z)_j^{n+1} - 2(\tilde{E}_z)_j^n + (\tilde{E}_z)_j^{n-1} + \Delta t^2 \lambda_j^2 (\tilde{E}_z)_j^n \\ = -\omega \Delta t^2 \cos(\omega t^n) \frac{1}{\epsilon} J_z,\end{aligned}\quad (62)$$

and

$$(\tilde{E}_z)_j^0 = \nu_j, \quad (\tilde{E}_z)_j^1 = (1 - \frac{1}{2} \lambda_j^2 \Delta t^2) \nu_j - \frac{\omega}{2} \Delta t^2 (\frac{1}{\epsilon} J_z)_j. \quad (63)$$

Following Appenndix B of [1], one can verify that

$$(\tilde{E}_z)_j^n = (\nu_j - \nu_j^\infty) \cos(\tilde{\lambda}_j t^n) + \nu_j^\infty \cos(\omega t^n), \quad (64)$$

where

$$\frac{\sin(\tilde{\lambda}_j \Delta t / 2)}{\Delta t / 2} = \lambda_j. \quad (65)$$

Let $\Pi_h \nu = \sum_j \bar{\nu}_j \psi_j$. Then, one can obtain

$$\bar{\nu}_j = \nu_j \beta_h(\tilde{\lambda}_j) + (1 - \beta_h(\tilde{\lambda}_j)), \quad (66)$$

where

$$\beta_h(\lambda) = \frac{2\Delta t}{T} \sum_{n=0}^M \eta_n \cos(\lambda t^n) \left(\cos(\omega t^n) - \frac{1}{4} \right). \quad (67)$$

Lemma 2.5 of [1] shows that $|\beta_h(\tilde{\lambda}_j)| \leq \rho_h := \max(1 - 0.3\delta^2, 0.63)$. Utilizing the fact that the composite trapezoidal rule is exact for pure periodic trigonometric functions of order less than the number of grid points, we complete the proof. \square

APPENDIX D

VERIFICATION OF TIME ERROR ELIMINATION IN YEE-EM-WAVEHOLTZ

With the modification in (35), $\tilde{\omega}$ in Theorem 1 becomes

$$\frac{\sin(\tilde{\omega} \Delta t / 2)}{\Delta t / 2} = \omega.$$

Meanwhile, (64) becomes

$$(\tilde{E}_z)_j^n = (\nu_j - \nu_j^\infty) \cos(\tilde{\lambda}_j t^n) + \nu_j^\infty \cos(\tilde{\omega} t^n), \quad (68)$$

and the original composite trapezoidal quadrature is no longer exact for $\nu_j^\infty \cos(\tilde{\omega} t^n)$. Hence, the modification (36) to the numerical quadrature is needed to eliminate time error from the numerical integration.

REFERENCES

- [1] D. Appelö, F. Garcia, and O. Runborg, "WaveHoltz: iterative solution of the Helmholtz equation via the wave equation," *SIAM Journal on Scientific Computing*, vol. 42, no. 4, pp. A1950–A1983, 2020.
- [2] A. Taflov and S. Hagness, *Computational electrodynamics: the Finite-Difference Time-Domain method*, 3rd ed. Artech House, 2005.
- [3] J. Hesthaven and T. Warburton, "Nodal high-order methods on unstructured grids: I. time-domain solution of Maxwell's equations," *J. Comput. Phys.*, vol. 181, pp. 186–221, 2002.
- [4] M.-O. Bristeau, R. Glowinski, and J. Périaux, "Controllability methods for the computation of time-periodic solutions; application to scattering," *Journal of Computational Physics*, vol. 147, no. 2, pp. 265–292, 1998.
- [5] M. J. Grote and J. H. Tang, "On controllability methods for the Helmholtz equation," *Journal of Computational and Applied Mathematics*, vol. 358, pp. 306–326, 2019.
- [6] M.-O. Bristeau, R. Glowinski, J. Périaux, and T. Rossi, "3D harmonic Maxwell solutions on vector and parallel computers using controllability and finite element methods," Ph.D. dissertation, INRIA, 1999.
- [7] D. Pauly and T. Rossi, "Theoretical considerations on the computation of generalized time-periodic waves," *arXiv preprint arXiv:1105.4095*, 2011.
- [8] J. Rabinä, S. Mönkölä, T. Rossi, A. Penttilä, and K. Muinonen, "Comparison of discrete exterior calculus and discrete-dipole approximation for electromagnetic scattering," *Journal of Quantitative Spectroscopy and Radiative Transfer*, vol. 146, pp. 417–423, 2014.
- [9] W. C. Chew, J.-M. Jin, and E. Michielssen, *Fast and efficient algorithms in computational electromagnetics*. Artech house, 2001.
- [10] F. P. Andriulli, K. Cools, H. Bagci, F. Olyslager, A. Buffa, S. Christiansen, and E. Michielssen, "A multiplicative Calderon preconditioner for the electric field integral equation," *IEEE Transactions on Antennas and Propagation*, vol. 56, no. 8, pp. 2398–2412, 2008.
- [11] A. Toselli and O. Widlund, *Domain decomposition methods-algorithms and theory*. Springer Science & Business Media, 2006, vol. 34.
- [12] S.-C. Lee, M. N. Vouvakis, and J.-F. Lee, "A non-overlapping domain decomposition method with non-matching grids for modeling large finite antenna arrays," *Journal of Computational Physics*, vol. 203, no. 1, pp. 1–21, 2005.
- [13] M. N. Vouvakis, Z. Cendes, and J.-F. Lee, "A FEM domain decomposition method for photonic and electromagnetic band gap structures," *IEEE Transactions on Antennas and Propagation*, vol. 54, no. 2, pp. 721–733, 2006.
- [14] Z. Peng, V. Rawat, and J.-F. Lee, "One way domain decomposition method with second order transmission conditions for solving electromagnetic wave problems," *Journal of Computational Physics*, vol. 229, no. 4, pp. 1181–1197, 2010.
- [15] Z. Peng and J.-F. Lee, "Non-conformal domain decomposition method with second-order transmission conditions for time-harmonic electromagnetics," *Journal of Computational Physics*, vol. 229, no. 16, pp. 5615–5629, 2010.
- [16] V. Dolean, M. J. Gander, S. Lanteri, J.-F. Lee, and Z. Peng, "Effective transmission conditions for domain decomposition methods applied to the time-harmonic curl-curl Maxwell's equations," *Journal of computational physics*, vol. 280, pp. 232–247, 2015.
- [17] Z. Peng, X.-c. Wang, and J.-F. Lee, "Integral equation based domain decomposition method for solving electromagnetic wave scattering from non-penetrable objects," *IEEE Transactions on Antennas and Propagation*, vol. 59, no. 9, pp. 3328–3338, 2011.
- [18] M. Bonazzoli, V. Dolean, I. Graham, E. Spence, and P.-H. Tournier, "Domain decomposition preconditioning for the high-frequency time-harmonic Maxwell equations with absorption," *Mathematics of Computation*, vol. 88, no. 320, pp. 2559–2604, 2019.
- [19] R. Hiptmair, "Multigrid method for Maxwell's equations," *SIAM Journal on Numerical Analysis*, vol. 36, no. 1, pp. 204–225, 1998.
- [20] J. Gopalakrishnan, J. E. Pasciak, and L. F. Demkowicz, "Analysis of a multigrid algorithm for time harmonic Maxwell equations," *SIAM Journal on Numerical Analysis*, vol. 42, no. 1, pp. 90–108, 2004.
- [21] P. Lu and X. Xu, "A robust multilevel method for the time-harmonic Maxwell equation with high wave number," *SIAM Journal on Scientific Computing*, vol. 38, no. 2, pp. A856–A874, 2016.
- [22] P. Tsuji and L. Ying, "A sweeping preconditioner for Yee's finite difference approximation of time-harmonic Maxwell's equations," *Frontiers of Mathematics in China*, vol. 7, no. 2, pp. 347–363, 2012.
- [23] P. Tsuji, B. Engquist, and L. Ying, "A sweeping preconditioner for time-harmonic Maxwell's equations with finite elements," *Journal of Computational Physics*, vol. 231, no. 9, pp. 3770–3783, 2012.

- [24] K. Yee, "Numerical solution of initial boundary value problems involving Maxwell's equations in isotropic media," *IEEE Transactions on antennas and propagation*, vol. 14, no. 3, pp. 302–307, 1966.
- [25] A. Taflove and S. C. Hagness, *Computational electrodynamics: the finite-difference time-domain method*. Artech house, 2005.
- [26] J. S. Hesthaven and T. Warburton, *Nodal discontinuous Galerkin methods: algorithms, analysis, and applications*. Springer Science & Business Media, 2007.
- [27] B. Cockburn, G. E. Karniadakis, and C.-W. Shu, *Discontinuous Galerkin methods: theory, computation and applications*. Springer Science & Business Media, 2012, vol. 11.
- [28] J. W. Banks, B. B. Buckner, W. D. Henshaw, M. J. Jenkinson, A. V. Kildishev, G. Kovačič, L. J. Prokopeva, and D. W. Schwendeman, "A high-order accurate scheme for Maxwell's equations with a generalized dispersive material (GDM) model and material interfaces," *Journal of Computational Physics*, vol. 412, p. 109424, 2020.
- [29] J. LaGrone and T. Hagstrom, "Double absorbing boundaries for finite-difference time-domain electromagnetics," *Journal of Computational Physics*, vol. 326, pp. 650–665, 2016.
- [30] Z. Sun and H. K. Kim, "Refractive transmission of light and beam shaping with metallic nano-optic lenses," *Applied Physics Letters*, vol. 85, no. 4, pp. 642–644, 2004.
- [31] L. Verslegers, P. B. Catrysse, Z. Yu, J. S. White, E. S. Barnard, M. L. Brongersma, and S. Fan, "Planar lenses based on nanoscale slit arrays in a metallic film," *Nano letters*, vol. 9, no. 1, pp. 235–238, 2009.
- [32] M. Seo, H. Park, S. Koo, D. Park, J. Kang, O. Suwal, S. Choi, P. Planken, G. Park, N. Park *et al.*, "Terahertz field enhancement by a metallic nano slit operating beyond the skin-depth limit," *Nature Photonics*, vol. 3, no. 3, pp. 152–156, 2009.
- [33] R. Meade, J. N. Winn, and J. Joannopoulos, "Photonic crystals: Molding the flow of light," 1995.

Daniel Appelö Bio: Daniel Appelö holds a Ms degree in Electrical Engineering and a Ph. D. degree in Numerical Analysis from the Royal Institute of Technology in Sweden and is currently an Associate Professor in the Department of Computational Mathematics, Science and Engineering and the Department of Mathematics at Michigan State University.

Zhichao Peng Bio: Zhichao Peng holds a Ph. D. degree in Mathematics from the Rensselaer Polytechnic Institute in Troy, NY, USA in 2020. He is currently a research associate in the Department of Mathematics at Michigan State University.